Summary of the 2020/2021 Asian Winter Monsoon

This report summarizes the characteristics of the surface climate and atmospheric/oceanographic considerations related to the Asian winter monsoon for 2020/2021.

Note: The Japanese 55-year Reanalysis (JRA-55; Kobayashi et al. 2015) atmospheric circulation data and COBE-SST (Ishii et al. 2005) sea surface temperature (SST) data were used for this investigation. NOAA Interpolated Outgoing Longwave Radiation (OLR) data (Liebmann and Smith 1996) provided by the U.S. NOAA Earth System Research Laboratory (ESRL) from their web site at https://www.esrl.noaa.gov/psd/ was referenced to infer tropical convective activity. The base period for the normal is 1981 to 2010. The term "anomaly" as used in this report refers to deviation from the normal.

1. Surface climate conditions

In winter 2020/2021, three-month mean temperatures were above normal from South Asia to East Asia and below normal from Central Asia to southern Siberia. Clear intra-seasonal temperature anomaly variations were seen from Central to East Asia, where temperatures were low or very low in December and high or very high in February (Figure 3-1). Thus, the East Asian Winter Monsoon (EAWM) was stronger than normal in the first half of winter 2020/2021 and weaker in the second half. Winter precipitation was above normal in and around southern Central Siberia and from the southern part of South Asia to central Southeast Asia, and below normal in and around southern Central Asia. The wetter-than-normal conditions observed in Southeast Asia were consistent with typical anomaly patterns observed in past La Niña events. Drier-than-normal conditions were observed from northern Central Asia to northwestern East Asia and in the eastern part of East Asia in December, while wetter-than-normal conditions were observed in February (Figure 3-2).

Figure 3-3 shows extreme climate conditions for the period between December 2020 and February 2021. Extremely high temperatures were seen from southern India to southwestern China in January and from northwestern South Asia to the eastern part of East Asia in February. Extremely low temperatures were seen in and around southern Central Asia and from Mongolia to northern China in December. Extremely high precipitation was observed in and around central Southeast Asia and southern India in January and from southern Western Siberia to southern Central Siberia in February. Extremely low precipitation was observed in and around the central part of Central Asia in December and in and around southern Central Asia in January.

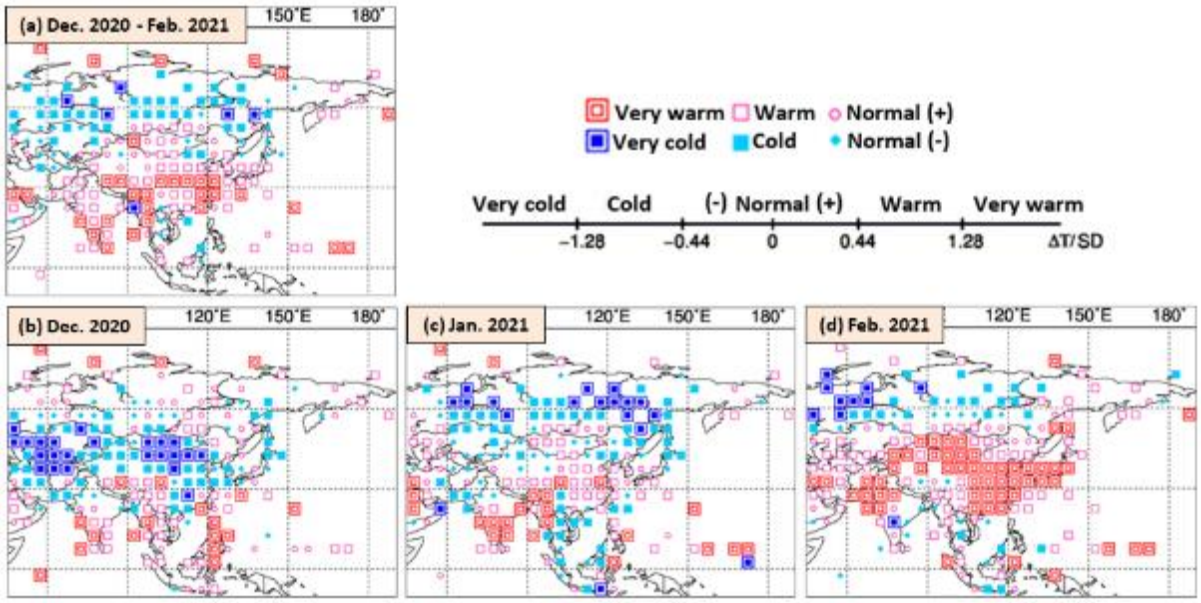

Figure 3-1 Temperature anomalies for (a) December 2020 to February 2021, (b) December 2020, (c) January 2021 and (d) February 2021

Categories are defined by the three-month/monthly mean temperature anomaly against the normal divided by its standard deviation and averaged in 5° × 5° grid boxes. The thresholds of each category are-1.28,-0.44, 0, +0.44 and +1.28. Standard deviations were calculated from 1981- 2010 statistics. Areas over land without graphical marks are those where observation data are insufficient or where normal data are unavailable.

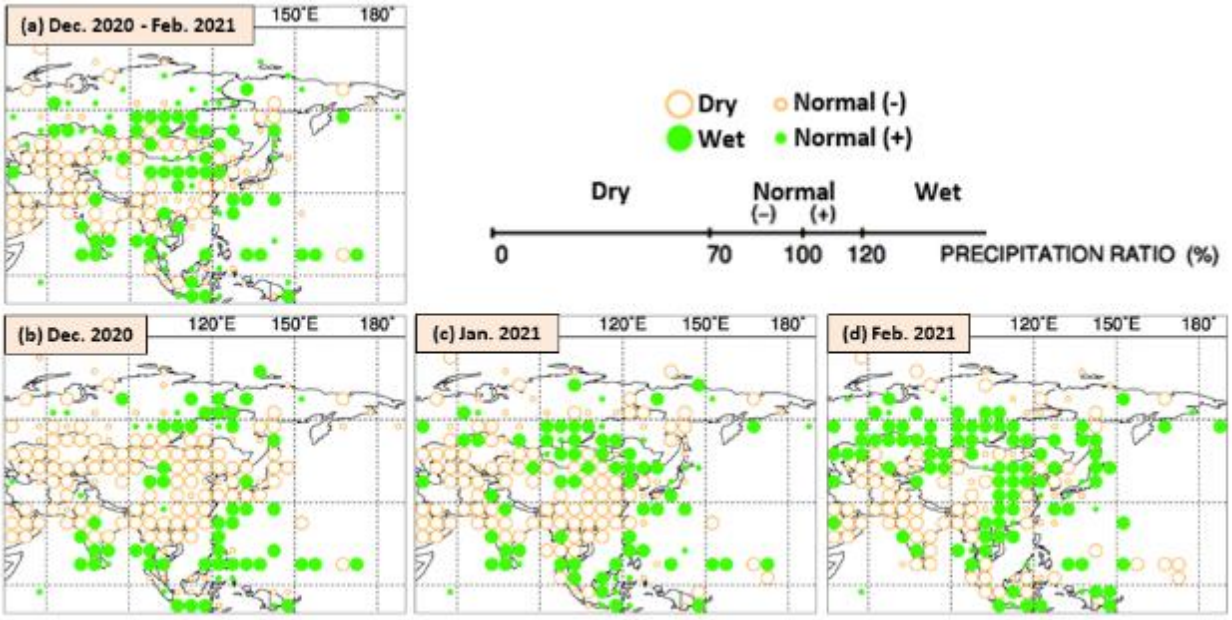

Figure 3-2 Precipitation ratio for (a) December 2020 to February 2021, (b) December 2020, (c) January 2021 and (d) February 2021

Categories are defined by the three-month/monthly precipitation ratio against the normal and averaged in 5° × 5° grid boxes. The thresholds of each category are 70, 100 and 120%. Areas over land without graphical marks are those where observation data are insufficient or where normal data are unavailable.

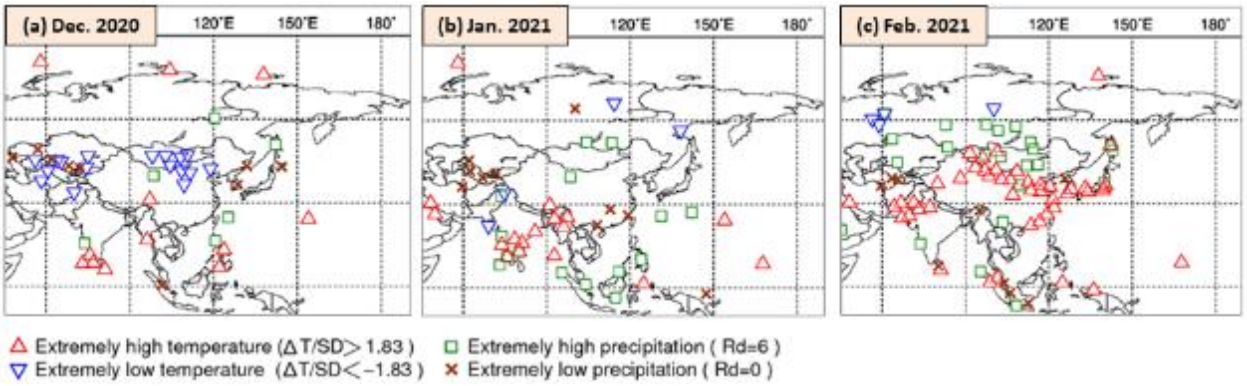

Figure 3-3 Extreme climate stations for (a) December 2020, (b) January 2021 and (c) February 2021

ΔT, SD and Rd indicate temperature anomaly, standard deviation and quintile, respectively.

2. Characteristic atmospheric circulation and oceanographic conditions

This section describes the characteristics of atmospheric circulation and oceanographic conditions in both halves of winter 2020/2021 against a background of distinct intra-seasonal EAWM change.

2.1 Conditions in the tropics

In the equatorial Pacific, remarkably positive SST anomalies were observed west of 150°E, and remarkably negative anomalies were observed from east of 160°E to the central part, in association with the La Niña event that had persisted since boreal summer 2020. In the Indian Ocean, positive SST anomalies observed from the central to eastern part of the northern tropical region and from the area near Madagascar to northwest of Australia decreased during winter (Figure 3-4 (a), (b)). Convective activity inferred from OLR in the first half of the season was enhanced from the central tropical Indian Ocean to the Maritime Continent, reflecting higher-than-normal SSTs in these regions, and was suppressed around the date line in the equatorial Pacific (Figure 3-4 (c)). In the second half of the season, enhanced convection was observed from the eastern part of the Maritime Continent to the Philippines (Figure 3-4 (d)).

Figure 3-5 shows 200- and 850-hPa stream function fields for the first and second halves of winter. In the first half, clear upper-level anti-cyclonic circulation anomalies were seen over southern Eurasia in response to enhanced convective activity from the central tropical Indian Ocean to the Maritime Continent, which enhanced Rossby wave propagation accompanying southward meandering of the subtropical jet stream (STJ) over the eastern part of East Asia (Figure 3-6 (a)). In the second half, the STJ meandered northward over the eastern part of East Asia (Figure 3-6 (b)). This meandering is partly attributed to enhanced convection from the eastern part of the Maritime Continent to the Philippines.

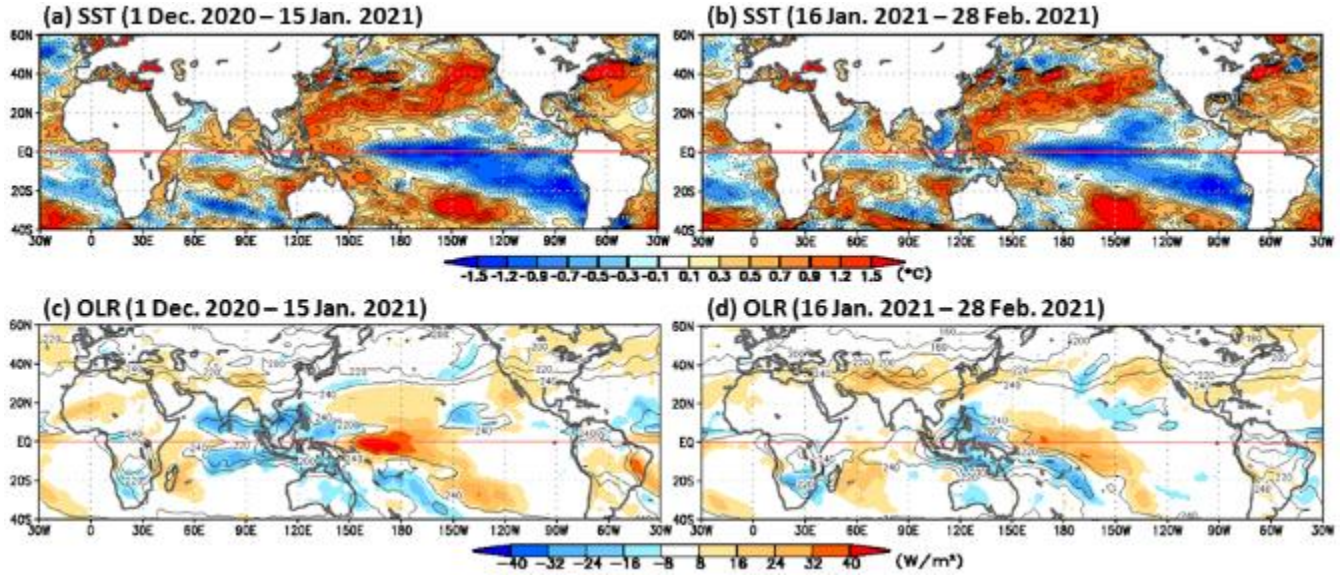

Figure 3-4 SST and OLR for 1 December 2020 to 15 January 2021 and 16 January to 28 February 2021

(a), (b) Shading shows SST anomalies [°C]. (c), (d) Contours indicate OLR at intervals of 20 W/m2, and shading shows OLR anomalies. Negative (cold color) and positive (warm color) OLR anomalies show enhanced and suppressed convective activity compared to the normal, respectively.

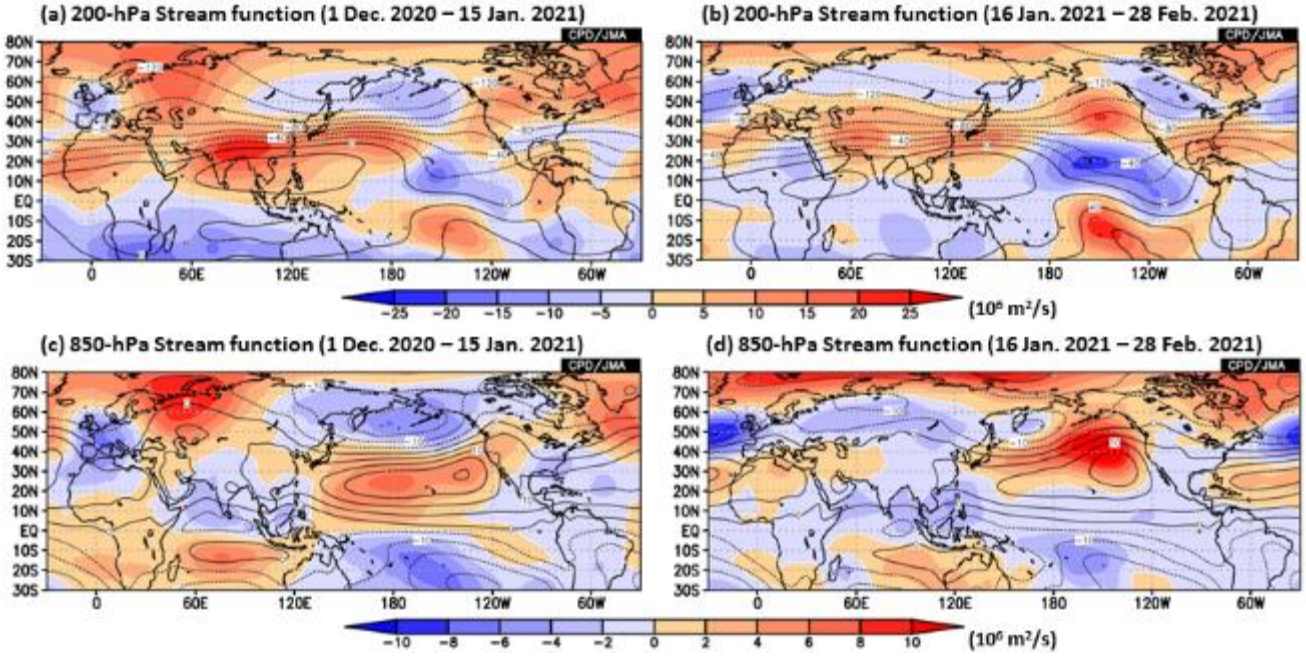

Figure 3-5 As per Figure 3-4, but for 200- and 850-hPa stream function

Contours indicate stream function at intervals of (a) (b) 20 × 106 m2/s and (c) (d) 5 × 106 m2/s, and shading shows stream function anomalies.

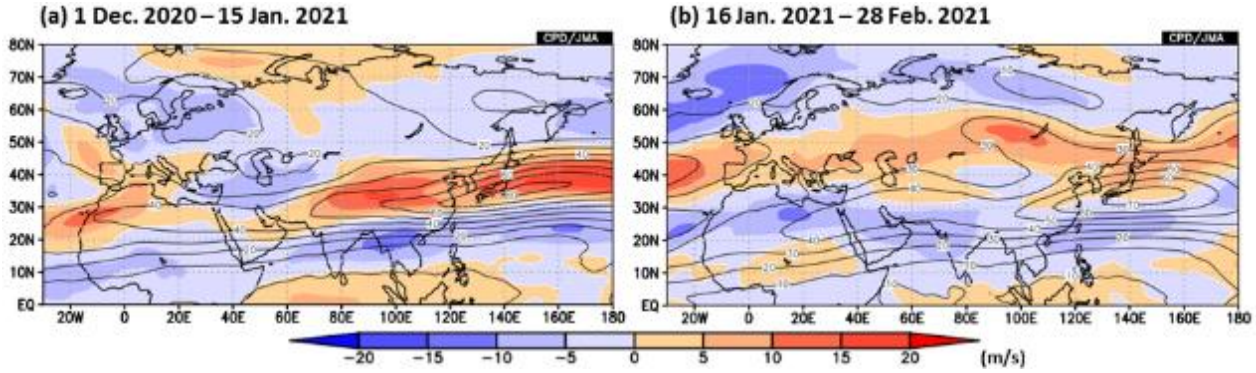

Figure 3-6 As per Figure 3-4, but for 250-hPa wind speed

Contours indicate wind speed at intervals of 10 m/s, and shading shows wind speed anomalies.

2.2 Conditions in the extratropics

The tropospheric polar vortex in the Northern Hemisphere was split into Siberian and North American parts throughout the winter. The polar front jet stream (PFJ) over Eurasia exhibited meandering in the first half of winter, but became clear and showed limited meandering near 50°N in the second half.

Figure 3-7 shows 500-hPa height and sea level pressure in the Northern Hemisphere. In the first half of the season there was a prominent wave train from the North Atlantic to northern Eurasia with a persistent blocking high over Western Siberia, which was possibly attributable to less-than-normal sea ice extents in the Barents Sea (e.g., Mori et al. 2014). Clear negative 500-hPa height anomalies were seen from northeastern East Asia to the northern North Pacific in association with the southward meandering of the PFJ over the region. Corresponding to these upper-level anomaly patterns, the Siberian High and the Aleutian Low were stronger than normal in sea-level pressure fields, indicating a stronger-than-normal EAWM. Lower-level tropospheric temperatures were below normal over eastern Eurasia (Figure 3-8 (a)).

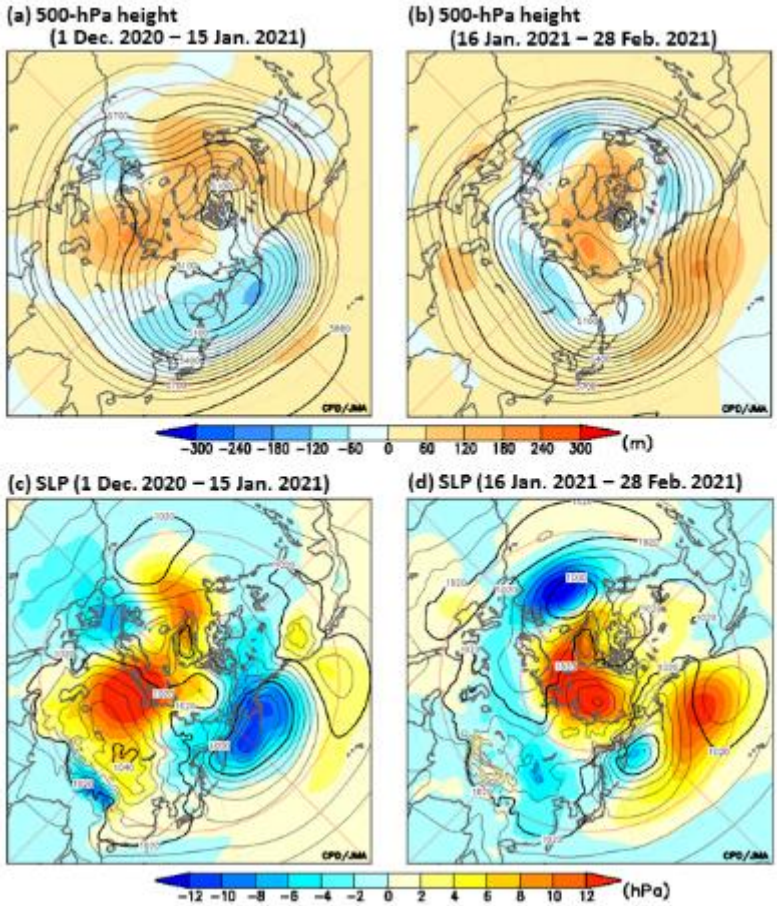

Figure 3-7 As per Figure 3-4, but for 500-hPa height and sea level pressure (SLP)

Contours indicate (a), (b) 500-hPa height at intervals of 60 m, and (c), (d) SLP at intervals of 4 hPa. Shading denotes related anomalies.

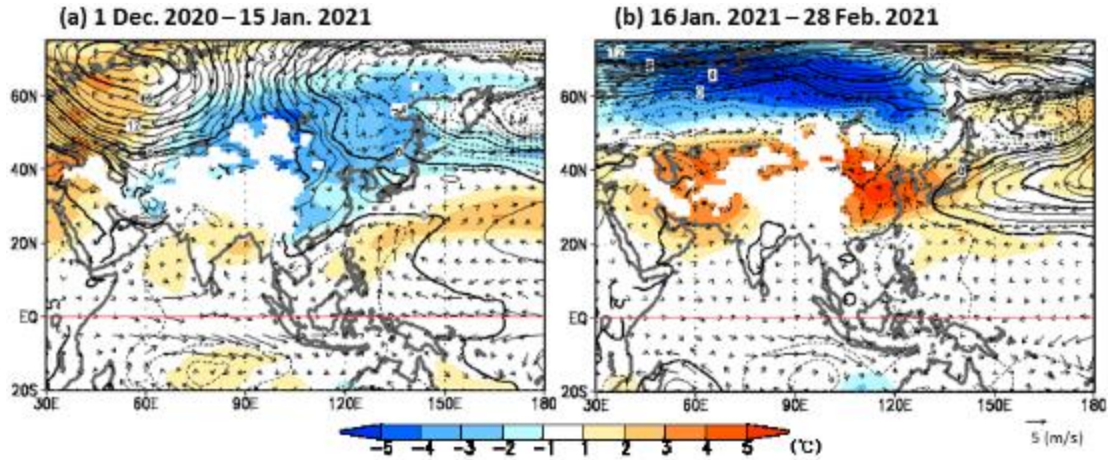

Figure 3-8 As per Figure 3-4, but for SLP anomalies, 850-hPa temperature anomalies and 925-hPa wind anomalies

Contours indicate SLP anomalies at intervals of 1 hPa, and shading shows 850-hPa temperature anomalies [°C]. Vectors denote 925-hPa wind anomalies [m/s].

In the second half of the season, zonally elongated positive anomalies were seen in 500-hPa height fields from southern Europe to East Asia, and negative anomalies were seen over northern Eurasia (Figure 3-7 (b)). Temperatures at 850 hPa were above normal over a wide area from Central to East Asia and below normal north of 50°N over Eurasia (Figure 3-8 (b)). These anomalies were consistent with a clear and non-meandering PFJ near 50°N over Eurasia (Figure 3-6 (b)), which may be linked to a stratospheric sudden warming event occurring from January to early February. In the sea level pressure field, the Siberian High was weaker than normal and the Aleutian Low was shifted northwestward of its normal position (Figure 3-7 (d)), indicating a weaker-than-normal EAWM that contributed to the warm conditions observed in Central and East Asia.

(SATO Hitoshi, Tokyo Climate Center)

References

Ishii, M., A. Shouji, S. Sugimoto and T. Matsumoto, 2005: Objective analyses of sea-surface temperature and marine meteorological variables for the 20th century using ICOADS and the Kobe Collection. *Int. J. Climatol.*, **25**, 865-879.

Kobayashi, S., Y. Ota, Y. Harada, A. Ebita, M. Moriya, H. Onoda, K. Onogi, H. Kamahori, C. Kobayashi, H. Endo, K. Miyaoka, and K. Takahashi, 2015: The JRA-55 Reanalysis: General specifications and basic characteristics. *J. Meteor. Soc. Japan*, **93**, 5 – 48.

Liebmann, B., and C. A. Smith, 1996: Description of a complete (interpolated) outgoing longwave radiation dataset. *Bull. Amer. Meteor. Soc.*, **77**, 1275–1277.

Mori, M., M. Watanabe, H. Shiogama, J. Inoue, and M. Kimoto, 2014: Robust Arctic sea-ice influence on the frequent Eurasian cold winters in past decades. *Nat. Geosci.,* **7**, 869-873.

<<Table of contents <Top of this article